Cement and Concrete Research 40 (2010) 1106–1113

Contents lists available at ScienceDirect

Cement and Concrete Research

journal homepage: http://ees.elsevier.com/CEMCON/default.asp

Monitoring evolution of compressive damage in concrete with linear and nonlinear ultrasonic methods

P. Antonaci [a], C.L.E. Bruno [a,*], A.S. Gliozzi [b], M. Scalerandi [b]

[a] Structural and Geotechnical Engineering Department, Politecnico di Torino, Corso Duca degli Abruzzi 24, 10129 Torino, Italy
[b] Physics Department, Politecnico di Torino, Corso Duca degli Abruzzi 24, 10129 Torino, Italy

ARTICLE INFO

Article history:
Received 1 December 2009
Accepted 26 February 2010

Keywords:
Characterization (B)
Mechanical properties (C)
Microcracking (B)
Degradation (C)
Concrete (E)

ABSTRACT

An experimental study was conducted on different concrete cylinders damaged in compression. The evolution of damage was followed by means of linear and nonlinear ultrasonic methods, with the purpose to provide a better understanding of mechanical degradation processes in concrete and highlight the potentialities and limitations of the Non-Destructive Techniques used.

1. Introduction

Although *in situ* tests can often offer only qualitative results, Non-Destructive Techniques (NDT) hold a very important role in architectural sciences and civil engineering, particularly when the evaluation of degradation of pre-existing structures and infrastructures is involved [1,2]. Due to the interaction between propagating elastic waves and properties of the medium, ultrasonic techniques, such as those based on the measurement of attenuation or pulse velocity, have been widely used in the last decades to evaluate the mechanical properties of cement-based materials [3,4].

Recent studies have highlighted the chance to define novel ultrasonic Non-Destructive Techniques by taking advantage of some peculiar features related to the nonlinear properties of damaged materials [5,6]. In particular, researchers have shown that the elastic excitation of cracks at the micro- or meso-scale can induce the generation of nonlinear terms in the wave propagating through the damaged element [5,7,8]. Being such terms specific of damage, i.e. not generated by heterogeneities or geometrical flaws of the sample, nonlinear ultrasounds can be more sensitive to the degradation of the materials' mechanical properties, yet in the early stages of damage [9]. Thus, improving experimental methods to properly excite a sample and extract the full nonlinear signature in the resulting ultrasonic output signal can lead to more effective diagnostic methods to test the integrity of the material.

In the present work, we intend to compare the performances of linear and nonlinear ultrasonic NDT in following the evolution of compressive damage in concrete specimens. Also, we aim to delineate the potentialities and possible limitations of the experimental methods used. In particular, on the basis of previous works [10,11], a specific protocol of nonlinear ultrasonic NDT, the Scaling Subtraction Method (SSM), will be introduced and compared to traditional harmonic analyses and to linear techniques such as attenuation measurements and pulse velocity detection. Results of the experiments conducted in this study will be shown to prove the intrinsic potential of the Scaling Subtraction Method if compared to classical linear and nonlinear techniques and its effectiveness in describing the damage process.

2. Nonlinear ultrasonic methods

As shown in previous works [9–11], the presence of micro- and meso-cracks in an elastic medium breaks the proportionality between an impinging ultrasonic wave and the corresponding elastic response of the medium. The break of proportionality can be retraced to three main mechanisms [11]:

1. Nonlinear losses of elastic energy.
2. Redistribution of energy among the various generated frequencies.
3. Dependence of the elastic constants on the excitation amplitude.

In general, the response $v_A(t)$ of a nonlinear sample excited by a sinusoidal monochromatic wave v_{inp} of amplitude A and frequency ω_0

* Corresponding author.
E-mail addresses: paola.antonaci@polito.it (P. Antonaci), caterina.bruno@polito.it (C.L.E. Bruno), antonio.gliozzi@polito.it (A.S. Gliozzi), marco.scalerandi@infm.polito.it (M. Scalerandi).

0008-8846/$ – see front matter © 2010 Elsevier Ltd. All rights reserved.
doi:10.1016/j.cemconres.2010.02.017

($v_{inp} = A \sin \omega_0 t$) can be written in terms of a Fourier Series expansion as follows:

$$v_A(t) = \sum_{n=1}^{\infty} B_n(A)[\sin(n\omega_0 t + \phi_n(A)]. \quad (1)$$

The three mechanisms listed above can be easily individuated in the expression of Eq. (1). In particular:

1. Nonlinear attenuation is described by the dependence of the coefficients B_n on the amplitude A of the injected signal. Indeed, while in a linear medium the amplitude of the response at the fundamental frequency can be written as $B_1(A) = \gamma A$ (linear attenuation, γ being a constant) such a relation is not valid in nonlinear media, where $B_1(A) < \gamma A$. Furthermore, the function $f(A) = \gamma A - B_1(A)$ is a function which increases with A, thus denoting an increase of losses with the increase of the exciting amplitude;
2. Generation of higher order harmonics is implicit in the summation;
3. Nonlinearity of the elastic constants is given by the dependence of the phases ϕ_n on the amplitude of the injected signal. Phases are related to the wave speed, which depends on the elastic constants. In most cases, damage is accompanied by softening, i.e. a phase delay (velocity reduction) is observed when the exciting amplitude increases.

Since an increase of the signature of nonlinearity is associated to an increase of damage, the goal of nonlinear ultrasonic methods is to extract the signature of the nonlinearity from the elastic response of the tested element to characterize damage progression. Here, we will compare two different nonlinear methods:

- Spectral analysis. Based on filtering techniques (e.g. Fast Fourier Transform [12], Phase Coded Subtraction Methods [13]), it allows to analyze the frequency content of the elastic response of the medium and to evaluate the amplitude of the newly generated higher order frequencies and their dependence on the amplitude of the fundamental frequency of the excitation.
- The Scaling Subtraction Method (SSM) [11]. Introducing the experimental definition of a (linear) reference signal, it allows to evaluate the total nonlinear content of the elastic response.

Note that other nonlinear methods, such as those based on measurements of the resonance frequency [14,15] or on the generation and detection of sub-harmonics [16] and sidebands [17], can be used for damage evaluation, but will not be discussed here.

2.1. Spectral analysis

Spectral analysis is a typical nonlinear ultrasonic technique [18–20]. As previously underlined, when exciting an elastic medium with a monochromatic wave, the interactions of the traveling wave with the nonlinear scatterers inside the medium (e.g. micro-cracks) give rise to new harmonic components. Accordingly, the nonlinear signature in spectral analysis is usually expressed as the amplitude of the second (β) or third (δ) harmonic as a function of the amplitude of the fundamental frequency. The frequency components are obtained by the analysis of the recorded temporal signals in the Fourier domain. In hysteretic media, such as concrete, this dependence of the β (δ) indicator is generally found to be different from the classical quadratic (cubic) power law [6].

In Fig. 1a, experimental results of one of the ultrasonic tests described in Section 4 are reported. In particular, results from sample B13 (undamaged state) are considered. The amplitude of the second harmonic (B_2) is plotted versus the amplitude of the fundamental component (B_1) of the output signal, at increasing excitation amplitudes. It has to be remarked that the amplitude recorded for the second harmonic component is very small, essentially due to the use of narrow-band transducers and to the relatively low resolution of the acquisition system used for the experiments. Nonetheless, it can still be detected, and similar results can be found for the third harmonic as well.

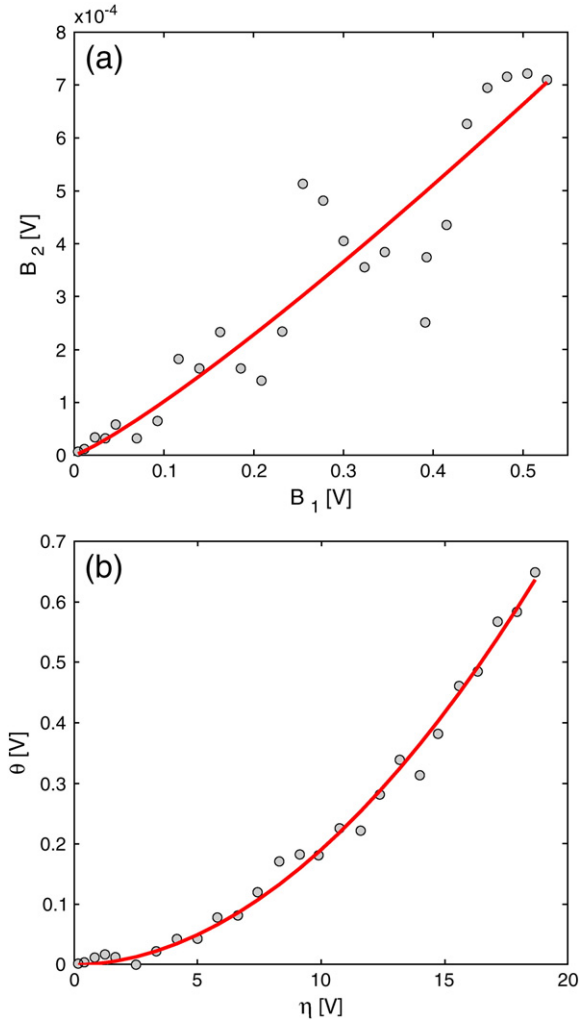

Fig. 1. Non linear ultrasonic measurements on sample B13 in the intact state. (a) Amplitude of the second harmonic versus the amplitude of the fundamental component. (b) SSM indicator θ. versus the maximum of the output a. Experimental data (circles) have been fitted by means of a power law function (solid line) as defined in Eqs. (2) and (7).

Data (circles) have been fitted by means of a power law function (solid line):

$$B_2 = \tilde{a}\left(\frac{B_1}{B_{ref}}\right)^{\tilde{b}} B_{ref}. \quad (2)$$

In Eq. (2) B_{ref} is a reference amplitude value ($B_{ref} = 0.1\ V$) used for normalization purposes; $\tilde{a}$ and $\tilde{b}$ are adimensional fitting parameters and in particular the following values have been found: $\tilde{a} = 10^{-3}$ and $\tilde{b} = 1.17$.

In the following, results concerning the spectral analysis will no longer be reported, since the evaluation of the quality of the technique is biased by the use of narrow-band transducers. Nevertheless, we remark that, even with the equipment used for our experiments, the second harmonic still provides a rough information about the progression of damage in a given sample. Therefore, we expect results from an accurate (in terms of equipment) harmonic analysis to be as good as those given by the SSM technique. The advantage of the SSM approach still remains, in our opinion, two-folds: on the technical side it presents less requirements about the quality of the instrumentation and on the mathematical side it is simpler to implement and does not need to introduce parameters such as those often required for a fast Fourier Transform.

2.2. The Scaling Subtraction Method

The Scaling Subtraction Method is based on the comparison between the recorded nonlinear signal $\upsilon_A(t)$, representing the elastic nonlinear response of a damaged element to a given excitation amplitude A, and a reference signal $\upsilon_{ref}(t)$. The latter is defined in a post processing analysis based on experimental data and represents the ideal linear elastic response of the same element to the same excitation amplitude if no damage had occurred. The definition of $\upsilon_{ref}(t)$ is based on the assumption that, when the sample is excited by a sufficiently low amplitude A_{lin}, nonlinear terms are negligible and the recorded signal, which is experimentally measured, can be considered as the linear elastic response of the specimen. The linear reference signal (υ_{ref}) at a higher amplitude $A = kA_{lin}$ ($k \gg 1$) is obtained by applying the proportionality principle, valid if the system was linear (i.e. not damaged). The elastic response expected from an equivalent linear sample to the same high amplitude excitation would then be:

$$\upsilon_{ref}(t) = k\upsilon_{lin}(t) \neq \upsilon_A(t) \tag{3}$$

where υ_A is the actual nonlinear signal at high amplitude, i.e. the one measured on the nonlinear sample excited at the large amplitude A.

Nonlinear features contained in the elastic response of the specimen, as defined by Eq. (1), can be easily extracted by subtracting the linear reference of Eq. (3) from $\upsilon_A(t)$. As a result, one obtains a signal $w_A(t)$ (SSM signal) which contains the whole nonlinear features:

$$w_A(t) = \upsilon_A(t) - \upsilon_{ref}(t). \tag{4}$$

In the experimental data presented here, it is the phase-shift mechanism that provides the most relevant contribution to nonlinearity, as illustrated in Fig. 2. The SSM signal $w_A(t)$ depends on the amplitude (A) of the injected wave.

In the following, the SSM nonlinear signature θ will be represented by means of the maximum of the SSM signal $w_A(t)$:

$$\theta(A) = \max |w_A(t)|. \tag{5}$$

Likewise, a variable that represents the maximum of the recorded output was defined as:

$$\eta(A) = \max |\upsilon_A(t)|. \tag{6}$$

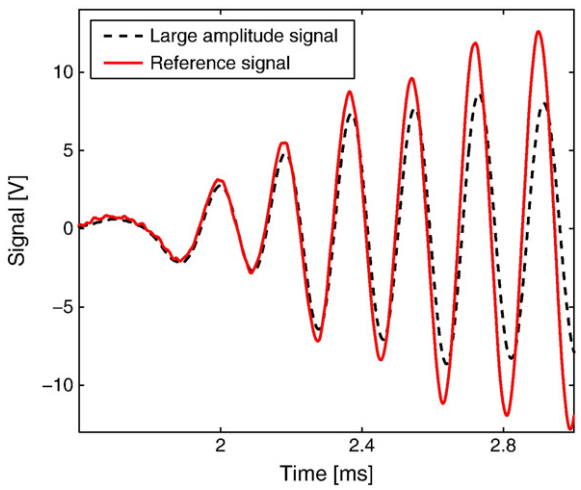

Fig. 2. Superposition of a portion of a nonlinear output signal (red solid line) at 25 V excitation amplitude (peak to peak, after amplification) and the corresponding portion of the related scaled linear reference signal (black dashed line).

In Fig. 1b, experimental results of one of the ultrasonic tests described in Section 4 are reported. In order to provide a clear view of the nonlinear signature evolution with the amplitude of the excitation, $\theta(A)$ is plotted as a function of $\eta(A)$. Here, the maximum of the recorded output $\eta(A)$ has been considered instead of the maximum of the injected input signal, since it was deemed more representative of the actual dynamic deformation process that takes place inside the material. Substantially identical results can be obtained when processing the experimental data in terms of signal "energy" instead of "maximum". Data (circles) have been fitted by means of a power law function (solid line):

$$\theta = a\left(\frac{\eta}{\eta_{ref}}\right)^b \eta_{ref} \tag{7}$$

with $\eta_{ref} = A_{lin}$, where A_{lin} is the lowest excitation amplitude ($A_{lin} = 0.25\ V$). Here, the fitting parameters have been found to be $a = 5 \cdot 10^{-4}$ and $b = 1.94$. Data refer to sample B13 in the intact state.

To clarify the role of the nonlinearity of the Young modulus and the attenuation in the definition of the signal $w_A(t)$, in Fig. 2 an example of temporal signals is reported. It can be seen that the reference signal (red solid line) differs from the large amplitude signal (black dashed line). In particular, as previously anticipated, we observe an increase in attenuation and a phase delay when the excitation amplitude is larger.

3. Linear ultrasonic methods

Linear ultrasonic methods are commonly used in Civil Engineering to evaluate the mechanical properties of concrete structures [21]. Typical linear ultrasonic methods consist in the measurement of the attenuation or the velocity of an ultrasonic wave traveling through the medium. Both methods have been applied to characterize damage in the test pieces examined in this study and will be briefly described in the following.

3.1. Attenuation

The attenuation of ultrasonic waves, which is in general due to absorption (e.g. transformation of elastic energy into heat) and scattering phenomena (e.g. diversion of the ultrasonic beam), is the decay rate of the energy of the elastic mechanical radiation as it propagates through the material. For what concerns absorption, in the 1-D case the linear attenuation coefficient ξ can be introduced by considering the decay of a wave traveling in the z direction:

$$u = u_0 e^{-\xi z} \tag{8}$$

where u is the reduced amplitude of the wave after it has traveled a distance z and u_0 is the amplitude of the wave at the initial location. Of course, the presence of damage affects the attenuating behavior of materials by increasing the energy losses, i.e. an increase of damage produces an increase of the attenuation coefficient ξ with consequent decrease of u.

In the following, we will refer to an attenuation indicator γ which has been calculated as the ratio of recorded output amplitudes over the injected amplitudes. Signals are recorded in a fixed position $z = z^*$. It follows that $\gamma = e^{-\xi z^*}$.

In Fig. 3, experimental results of one of the ultrasonic tests described in Section 4 are reported as points in the maximum of the output versus maximum of the input amplitude space. Notice that attenuation is calculated on the same set of signals recorded for the SSM analysis. Data (circles) have been fitted by means of a linear function (solid line):

$$\eta = \gamma A \tag{9}$$

where the coefficient γ is the attenuation indicator.

As previously discussed, this dependence is nonlinear for a damaged material, due to nonlinear attenuation mechanisms. Therefore, to make

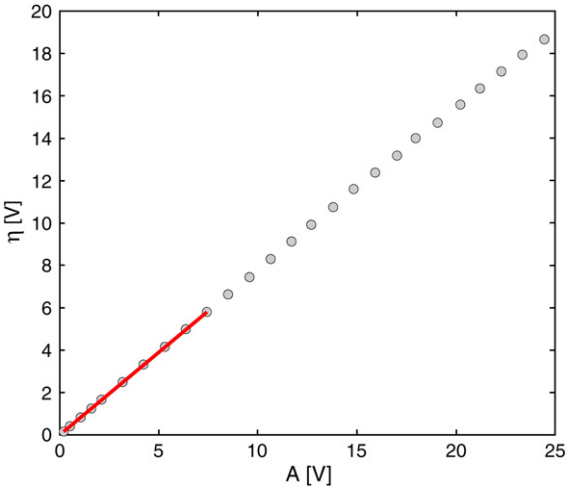

Fig. 3. Maximum of the output amplitude (after amplification) versus maximum of the input amplitude (after amplification) on sample B13 in the intact state. By fitting experimental data (circles) in the linear regime, the attenuation indicator γ was calculated as the direction coefficient of the fitting function.

sure that measurements were carried out in a linear regime, only low amplitudes up to approximately 8 V have been fitted as shown in Fig. 3. Data refer to sample B13 (undamaged state) and the following value of the fitting parameter was found: $\gamma = 0.78$.

Note that for the case reported in Fig. 3 nonlinearity in attenuation is almost not detectable (at least in the range of excitations considered), as it should be expected since the sample is in its intact state. We remark however that for damaged samples (particularly with increasing damage), the curve bends with downward concavity, thus manifesting an increase of both the linear and nonlinear contributions to attenuation (not reported).

3.2. Pulse velocity

Pulse velocity measurements are based on the relation between the velocity of the traveling wave and the elastic constants of the medium:

$$c_l = \sqrt{\frac{E_d(1-\upsilon)}{\rho(1+\upsilon)(1-2\upsilon)}} \tag{10}$$

where c_l is the wave speed of longitudinal waves, E_d is the dynamic modulus of elasticity and υ is the dynamic Poisson's ratio. Since density of the medium (ρ) is assumed to be constant, a decrease in the wave velocity is associated to a decrease of the elastic constants.

The wave speed can be easily calculated by:

$$c_l = \frac{s}{t} \tag{11}$$

where s is the traveled space and t is the Time Of Flight (TOF) of the traveling wave. Known the distance s between transducers, pulse velocity has been calculated by measuring the TOF t by means of a commercial device. Signals analyzed for the pulse velocity calculation are different from those used in the previous methods (spectral analysis, SSM and attenuation). The excitation was a pulse signal at a fixed amplitude.

4. Experiments

4.1. Experimental set-up

Linear (attenuation and pulse velocity) and nonlinear (SSM and spectral analysis) ultrasonic measurements were performed using the following testing equipment:

- Two identical piezoelectric transducers with a diameter of 40 mm and working frequency of 55.5 kHz. One was used as emitting source and the other one as receiver.
- An arbitrary waveform generator (Agilent 33220A), used to drive the emitting source, forcing it to vibrate according to a burst law of 10 sinusoidal cycles at a frequency of 55.5 kHz. The amplitudes of the input signals thus generated were controlled in order to be progressively increasing.
- A high voltage linear amplifier (FLC Electronics A400DI), enabling a 20× amplification factor.
- A data acquisition unit, equipped with an oscilloscope (Agilent Infinium DSO8064A) for real-time data visualization. Signals were recorded with a sampling rate of 10 MSa/s, that enabled a fairly accurate signal reconstruction, in accordance with Nyquist's theorem. Basically, Nyquist's theorem shows that a band limited analog signal can be perfectly reconstructed from an infinite sequence of samples if the sampling rate exceeds $2B$ samples per second, where B is the highest frequency in the original signal. This condition is fulfilled using the acquisition settling above illustrated. In addition, signals were recorded at specific dynamic ranges, adjusted in order to minimize the quantization error within the bounds of the acquisition system.
- A compact TOF device (Matest C370) equipped with an impulse generator, a synchronizer and a time counter, able to calculate the traveling time between the transmitting and receiving transducers. The embedded pulse generator of the device worked with an 800 V (peak to peak) excitation.

Linearity of the testing apparatus in working conditions was carefully verified in order to avoid any possible spurious effect that could alter the experimental observations. In particular, transducers were attached to the faces of each specimen through a thin layer of phenyl salicylate, whose linearity was preliminary verified using a reference linear (steel) sample. Analogously, linearity of the transducers' response in terms of vibration amplitude with increasing applied voltage was verified by using them coupled to the reference linear sample and ascertaining that excellent proportionality between input and output was obtained for any excitation amplitude.

4.2. Specimens and damage process

Eight cylindrical specimens (160 mm length and 60 mm diameter) were extracted from a concrete slab whose composition is detailed in Table 1.

A specific damage process was induced by applying a mono-axial compressive load along the longitudinal direction of the specimen through a 250 kN Mechanical Testing System, working under controlled displacement velocity. For each specimen, rupture load was reached through a number of loading steps at increasing intensity. The failure load of each specimen was ascertained at the end of the US tests and ranged between 100 kN and 120 kN.

Table 1
Details of the composition of the concrete mix.

Component type	Dosage
CEM II A-L 42.5 R	340 kg/m^3
Sand (0–5 mm)	957 kg/m^3
Gravel (5–15 mm)	846 kg/m^3
Water	200 kg/m^3
Admixtures	–
W/C ratio	0.59

All specimens were tested by means of linear and nonlinear ultrasonic NDT at the end of each load level and in their undamaged state, according to the procedure described in the following section.

4.3. Experimental procedure

For each sample, each set of measurements, e.g. one per each load level with the specimen removed from the loading frame, was performed as follows:

1. Injection of a sinusoidal burst at a low amplitude A_1.
2. Recording of the corresponding elastic response $v_{A_1}(t)$.
3. Steps 1 and 2 were repeated for increasing amplitudes A_i where $i=2, \ldots, 30$.
4. Time of Flight measurement at fixed (low) amplitude.

For what concerns steps 2 and 3, the amplitude of the excitation was varied between 1 V and 400 V peak to peak (after amplification). The recorded temporal signals were processed to estimate the SSM indicator θ, the harmonics content β and the attenuation indicator γ, as previously discussed. Furthermore, each measurement at step 2 was repeated nine times, each time after removing and re-attaching transducers. This was done in order to simulate realistic on-site testing conditions: for on-site assessment of full-scale structures, indeed, it could be required to remove the instrumentation after a first experimental examination and to repeat the measurements at prescribed time intervals. The possible variability to be ascribed to the removing/re-attaching procedure has been consequently evaluated in this study. The variability due to ordinary fluctuations of the environmental conditions during testing is also included. Indeed, no control of temperature and humidity conditions has been imposed in this study and the corresponding values ranged between 22–26 and 31–48°C respectively.

Time of Flight measurements (step 4) were repeated 100 times and the average value was calculated.

5. Sensitivity of the scaling subtraction method

In this section, we will present some results concerning the application of the SSM with the aim to prove its repeatability and sensitivity to the progression of damage. As it will be shown later, this approach seems to be the most complete for the purpose of detection and monitoring of damage.

The behavior of the SSM indicator θ as a function of the maximum of the output (η) at the end of different intensity loadings is analyzed in Fig. 4 for two of the eight samples. Notice that only a few loadings are represented in Fig. 4. Here, experimental data for each of the nine repeated measurements (symbols) are reported, together with the corresponding fitting functions (light solid lines), see Eq. (7). Furthermore, for each load level the average curve (calculated from the nine repeated measurements) was introduced and reported as a solid line in the plot, with error bars estimated from standard error theory. Notice that the repeated measurements are arranged in bands, thus showing good repeatability. Also, bands corresponding to different load levels are distinguishable one from the other. In particular, there is no superposition of error bars between averaged curves at different loads, thus proving the sensitivity of the method to the variations of the damaged state. As expected, the increase of load applied on the sample corresponds to the increase of the nonlinear parameter θ, thus showing progression of micro-cracks.

In addition, experimental results from all the tested specimens at zero load level (i.e. in the undamaged state) were superposed to verify that the initial undamaged state was comparable in all test pieces. As reported in Fig. 5, superposition of experimental data shows that all curves (data refer to four of the eight specimens, unloaded state) fall in a bunch well below the θ curve corresponding to a generic first load step (in particular, the red solid line on the plot corresponds to sample B10 at

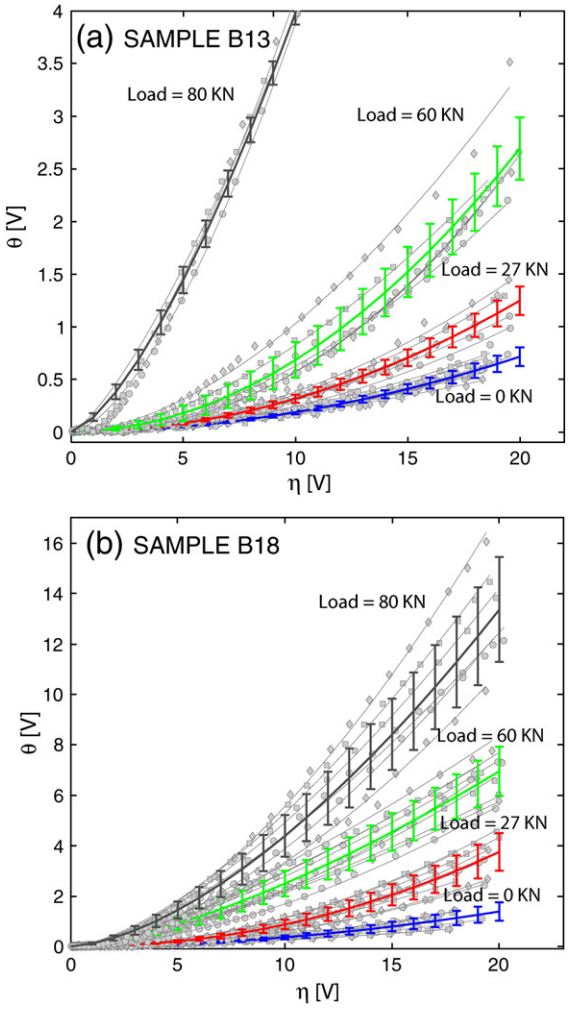

Fig. 4. SSM indicator (θ) versus maximum of the recorded output signal (η) for few loads. Results from specimens B13 and B18 are reported. For each load level, experimental data of the nine repeated measurements are reported (symbols) together with the corresponding fitting function (light solid lines). The solid line curve is obtained by averaging the nine sets of data.

27 kN load). In other terms, this result reveals that the variability of the SSM measurements on different specimens, due to the intrinsic heterogeneity of concrete, is sufficiently low to allow discrimination among successive load steps/damaged states, already at very low load levels.

Fig. 6 shows the curves of the SSM indicator θ, at each load step for three different specimens, as a function of the maximum of the recorded output signal. Notice that, in all cases, an increase of load corresponds to an increase of θ for a fixed value of η. Different specimens seem to have slight differences in the damage evolution. In particular, specimen B18 (Fig. 6c) shows a regular increase of nonlinearity, while for specimens B05 (Fig. 6a) and B13 (Fig. 6b) curves group into bunches, thus suggesting that damage progresses through different stages, as it will be discussed in the next section.

6. Damage indicators and efficiency of the ultrasonic techniques

As discussed in the previous sections, different techniques have been used to analyze ultrasonic data recorded on each sample. In particular, for each load level the average of nine repeated measurements have led to the curves of θ versus η (SSM indicator versus maximum of the output) and η versus A (maximum of the output versus maximum of the input). To

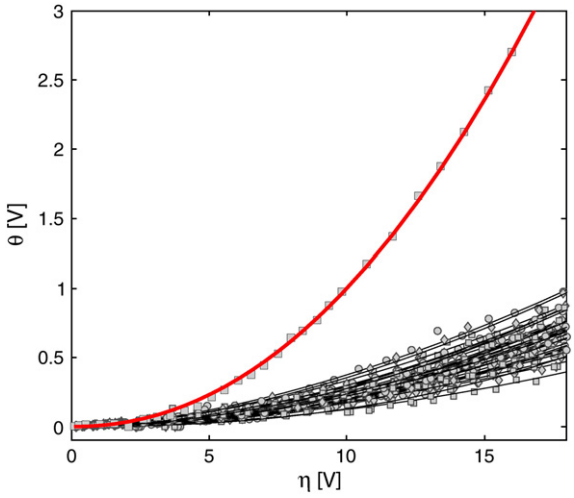

Fig. 5. SSM indicator (θ) versus maximum of the recorded output signal (η). Experimental data of the SSM tests on four specimens in the undamaged state have been superposed to show that they all group in a bunch. Notice indeed that data are very well distinguishable from the solid line representing the average curve corresponding to the first load step (27 kN) on one of the samples (B10).

extract information on damage from such curves, three damage indicators have been defined:

1. α: SSM nonlinear indicator. It is defined as the value of θ at a fixed value of $\eta = \eta_0 = 10$ V:

$$\alpha = \theta(\eta_0). \tag{12}$$

The value of α has been extrapolated from the average fitting functions in the form of Eq. (7). No qualitative changes occurred when varying the value of η_0.

2. γ: linear attenuation indicator. It is defined as the coefficient of the fitting function of Eq. (9);
3. c_l: pulse velocity linear indicator. It is defined as the wave speed measured in the sample at the given load.

Similarly, a harmonics nonlinear indicator λ could be defined on the basis of the measured harmonics content β. As remarked, λ, as calculated from the experimental results obtained in this study, does not show any significant variation as a function of load due to the large error bars. This has to be ascribed to the very low amplitude of the harmonic components, which, indeed, are almost submerged within noise level. Evidently, the use of narrow-band transducers, such as the ones used here, has a relevant role in the low resolution of higher order harmonics and the low quality of results from spectral analysis can be thus ascribed to this experimental set-up limitation. Indeed, good results have been obtained in the detection and monitoring of damage by other authors using spectral characterization [22,23]. For this reason, it was decided not to present the results related to the Harmonics Analysis and to focus on the comparative evaluation of the SSM with respect to the attenuation and pulse velocity methods only.

Fig. 7 reports the three indicators as a function of the applied load, normalized to the actual (*a posteriori*) failure load of the specimen, with reference to sample B13. The nonlinear SSM indicator α is plotted in Fig. 7a: nonlinearity of the sample increases with the increase of load and the growth rate is not constant. On the contrary, the linear indicators (γ and c_l, sub-plots in Fig. 7b and c) decrease almost linearly with load, until failure of specimens occurs. Notice that attenuation increases with load (γ decreases) while wave speed decreases, thus indicating a softening of the material, as expected.

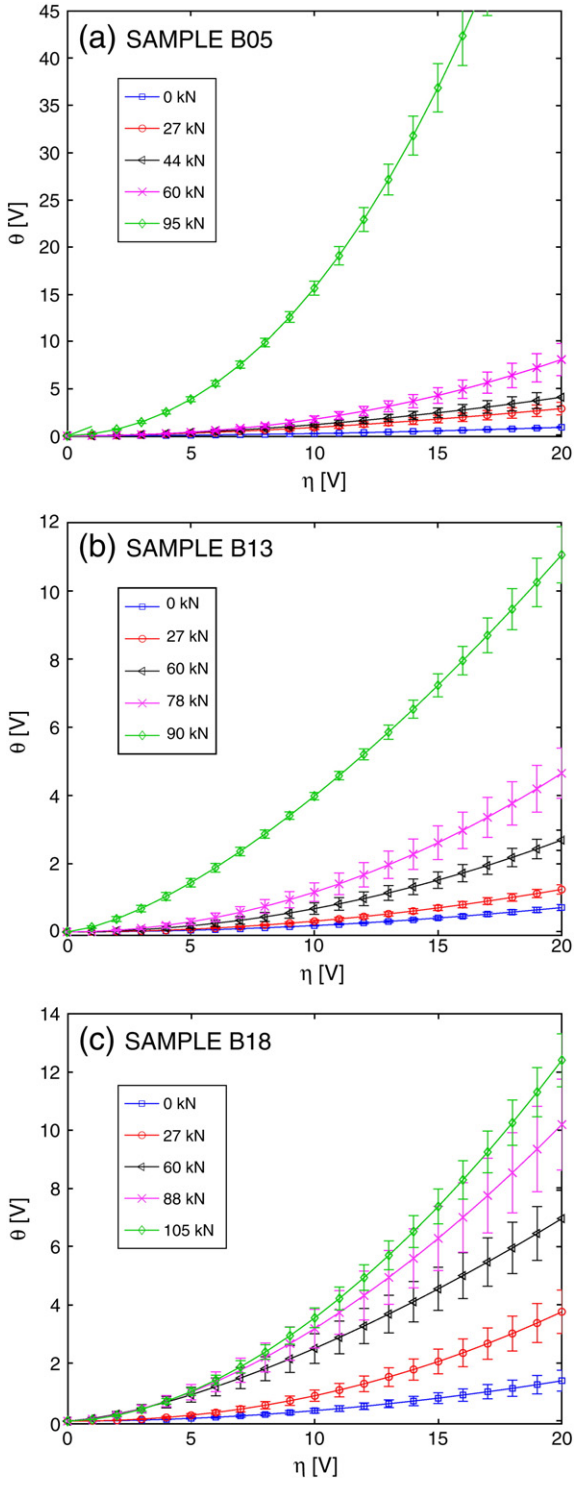

Fig. 6. SSM indicator (θ) versus maximum of the recorded output signal (η). Notice that nonlinearity always increase with the increase of load. Results for three samples are reported.

According to the results reported in Fig. 7, the SSM nonlinear indicator seems to offer some advantages in monitoring damage evolution. In fact, damage induced by quasi-static load is not expected to have a uniform growth. The existence of different phases in damage evolution is consistent with results from other techniques used in monitoring the progression of damage in concrete, such as for fatigue load [24–26]. Indeed, the SSM indicator (Fig. 7a) allows to distinguish

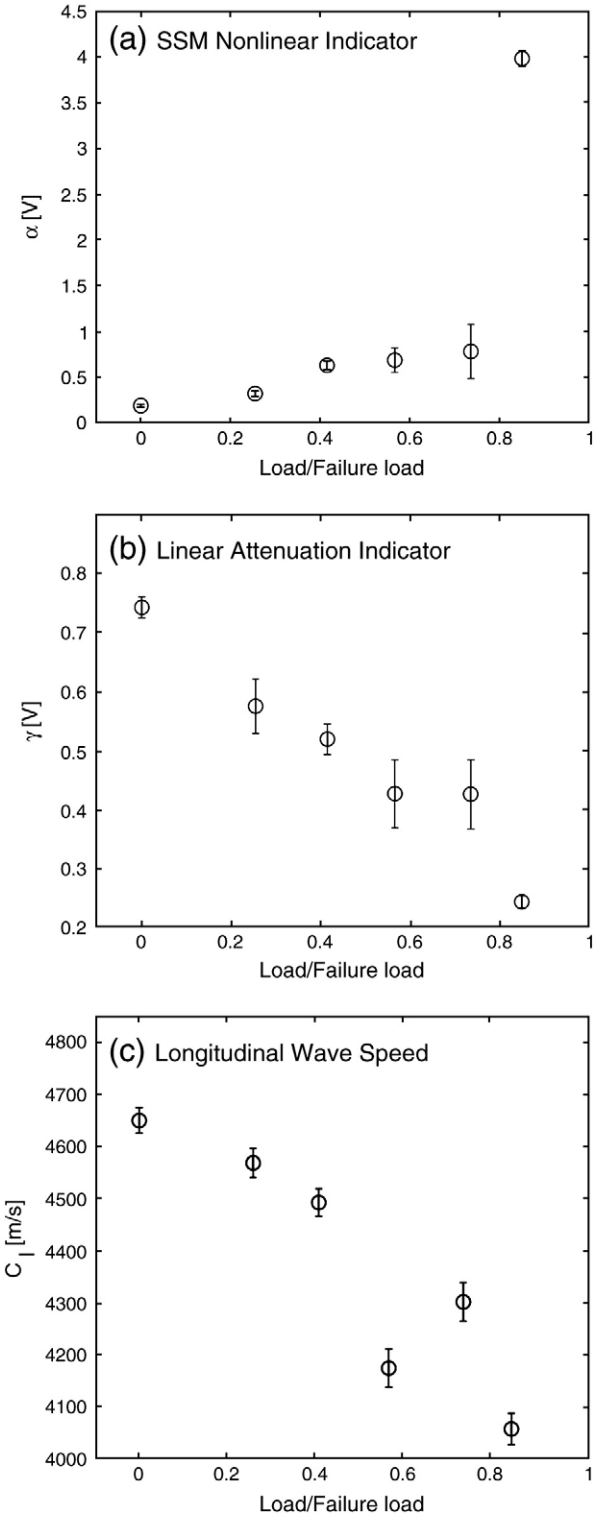

Fig. 7. Ultrasonic indicators of damage as a function of the applied load normalized to the actual rupture load. Results from sample B13 are reported. (a) Nonlinear SSM indicator α; (b) linear attenuation indicator γ; (c) linear wave speed indicator c_l. Notice that attenuation and pulse velocity show a linear dependence on the load while the nonlinear SSM indicator θ shows that different stages occur in the progression of damage.

three stages in the evolution of damage, none of which is enlightened by the linear indicators:

1. 0 to 30% of the failure load: early damage occurs, with formation of micro-cracks and a sudden change of the performances of the material.
2. 30% to 70% of the failure load: micro-cracks begin to coalesce in larger cracks and only a few new micro-cracks are formed. This corresponds to a slight increase of the nonlinearity, with consequent moderate decrease of the performances of the material;
3. 70% to failure: micro-cracks coalesce into macro-cracks. The SSM indicator suddenly increases. The rapid increase of α can be interpreted as an indication of imminent failure. Notice that linear indicators γ and c_l do not show any similar precursor sign.

Finally, the relative damage indicators have been defined as the percentage variation of the indicators described above, measured at each load (damage) level, with respect to the value of the same indicator at zero load level, i.e. in the undamaged condition. In symbols:

$$\frac{|\Delta\epsilon|}{\epsilon_0} = \frac{|\epsilon_i - \epsilon_0|}{\epsilon_0} \tag{13}$$

where ϵ stands for any of the linear or nonlinear indicators, α, γ and c_l while $i = 0, \ldots, M$ is the index representing the load level.

Fig. 8 shows the percentage variation of the measured indicators, as a function of the relative load, as defined above. Here, results for all the eight samples have been reported. While none of the two linear indicators give any information on the different stages of the evolution of damage, more details emerge from the SSM analysis of data (Fig. 8a). Indeed, the superposition of results from different specimens not only confirms the presence of different stages in damage evolution, but also, thanks to the repeatability of data, allows to describe the evolution of damage. Indeed, a fitting function able to describe the growth of nonlinearity has been found in the following:

$$\frac{|\Delta\alpha|}{\alpha_0} = a\left(1 - e^{(-L/b)} + ce^{((L-d)/f)}\right) \tag{14}$$

where L = load/failure load and a, b, c, d, and f are adimensional fitting parameters. In particular, the following values were found: $a = 5.86$, $b = 0.44$, $c = 4.58$, $d = 0.79$, and $f = 0.08$.

The nonlinear SSM technique points out the distinction between the initial degradation and the late propagation through a semi-stable stage where damage increases very slightly. A relevant aspect of data plotted in Fig. 8a is also that all experimental data follow the same trend when plotting the relative change in the nonlinear indicator, thus opening a door on a possible interpretation of damage evolution under compressive load.

Linear attenuation and pulse velocity measurements (respectively reported in sub-plots in Fig. 8b and c), as previously discussed, only show that the insurgence and the progression of damage has a linear dependence on the relative load. Indeed, in both cases experimental data have been fitted by means of a linear function:

$$\frac{|\Delta\epsilon|}{\epsilon_0} = a + bL \tag{15}$$

where L is the load level expressed as the percentage over the failure load and a and b are fitting parameters. For linear attenuation, the fitting parameters were found to be $a = 0.06$ and $b = 0.78$, while for pulse velocity the fitting parameters were $a = 0.1$ and $b = -0.142$.

7. Conclusion

The experimental study here presented made it possible to compare the performances of different linear and nonlinear ultrasonic NDT in evaluating damage evolution in concrete under compressive loads. In particular, the Scaling Subtraction Method, which is a simple nonlinear NDT, has been demonstrated to be reliable and very sensitive in the detection of damage and in monitoring its evolution. It has revealed, at least with the normally used *in situ* equipment, to be more efficient than traditional linear and other nonlinear techniques in as much as it points

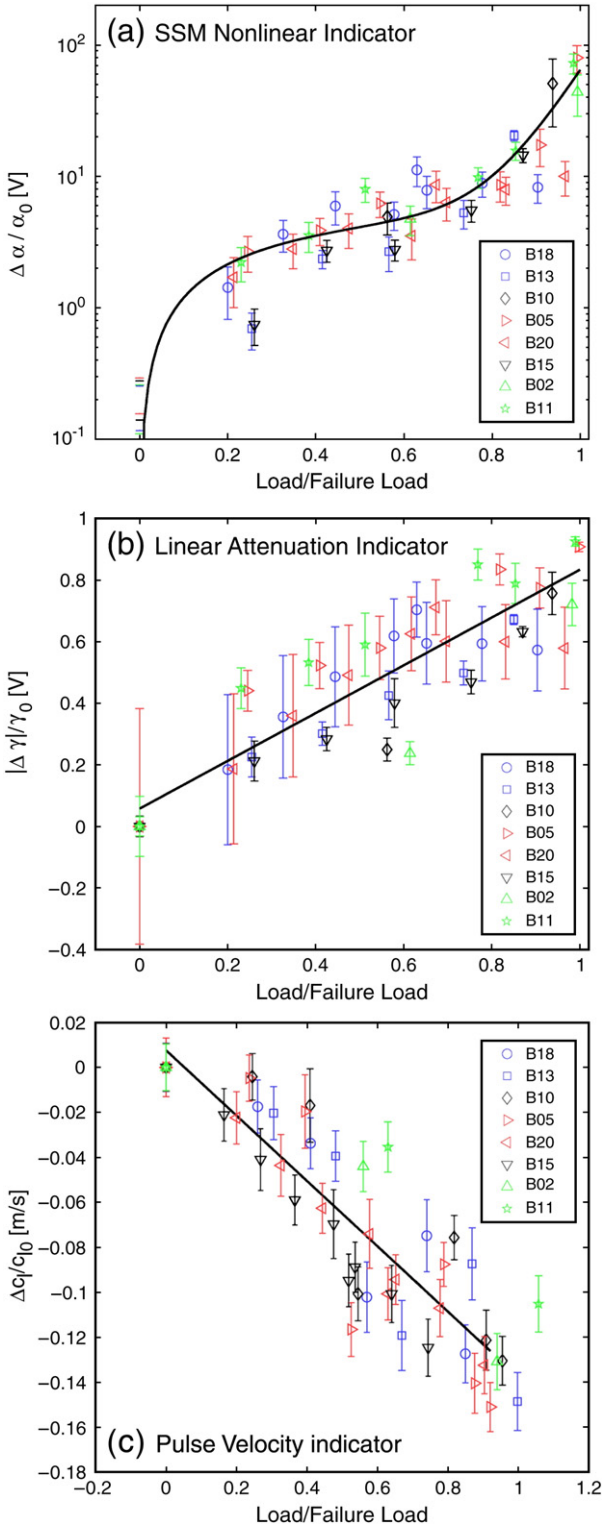

Fig. 8. Superposition of results from different specimens. (a) The variation of α for different specimens leads to the definition of a curve that describes the different stages of damage evolution. (b) and (c) point out that linear indicators show a linear evolution of damage.

out the distinction between initial stages of degradation and late damage propagation, highlighting the presence of an intermediate semi-stable stage. However, although very promising in terms of potential applications for *in situ* testing, the SSM still needs further development to solve technical issues related to the assessment of full-scale structures. In particular, a proper definition of the excitation frequency is required to overcome difficulties related to material attenuation properties. Also, the effectiveness of the method with regard to different types of damage (such as fatigue damage or chemical–physical degradation, etc.) should be investigated. Lab experiments are currently being performed to explore these issues and we expect the SSM to be efficient also in these cases, with further improvement expected to be obtained based on the investigation about the possible existence of critical thresholds.

Acknowledgement

Financial support by the Italian Ministry of Education, University and Research (Grant no. 20077ESJAP003) is gratefully acknowledged.

References

[1] D.M. McCann, M.C. Forde, Review of NDT methods in the assessment of concrete and masonry structures, NDT E Int. 34 (2001) 71–84.
[2] A. Carpinteri, S. Invernizzi, G. Lacidogna, *In situ* damage assessment and nonlinear modelling of a historical masonry tower, Eng. Struct. 27 (2005) 387–395.
[3] H.Y. Qasrawi, Concrete strength by combined nondestructive methods simply and reliably predicted, Cem. Concr. Res. 30 (2000) 739–746.
[4] B.C. Kim, J.Y. Kim, Characterization of ultrasonic properties of concrete, Mech. Res. Commun. 36 (2009) 207–214.
[5] R. Guyer, P.A. Johnson, Nonlinear mesoscopic elasticity: evidence for a new class of materials, Phys. Today 52 (4) (1999) 30–36.
[6] L.A. Ostrovsky, P.A. Johnson, Dynamic nonlinear elasticity in geomaterials, Riv. Nuovo Cim. 24 (7) (2001) 1–46.
[7] K. van den Abeele, J. De Vissche, Damage assessment in reinforced concrete using spectral and temporal nonlinear vibration techniques, Cem. Concr. Res. 30 (9) (2000) 1453–1464.
[8] M. Bentahar, H. El Aqra, R. El Guerjouma, M. Griffa, M. Scalerandi, Hysteretic elasticity in damaged concrete: quantitative analysis of slow and fast dynamics, Phys. Rev. B 73 (1) (2006) 014116.
[9] P. Antonaci, C.L.E. Bruno, P.G. Bocca, M. Scalerandi, A.S. Gliozzi, Nonlinear ultrasonic evaluation of load effects on discontinuities in concrete, Cem. Concr. Res. 40 (2) (2010) 340–346.
[10] M. Scalerandi, A.S. Gliozzi, C.L.E. Bruno, D. Masera, P.G. Bocca, A scaling method to enhance detection of a nonlinear elastic response, Appl. Phys. Lett. 92 (10) (2008) 101912(1–3).
[11] C.L.E. Bruno, A.S. Gliozzi, M. Scalerandi, P. Antonaci, Analysis of elastic nonlinearity using the Scaling Subtraction Method, Phys. Rev. B 79 (6) (2009) 064108(1–13).
[12] C. Payan, V. Garnier, J. Moysan, Effect of water saturation and porosity on the nonlinear elastic response of concrete, Cem. Concr. Res. 40 (3) (2010) 473–476.
[13] T. Goursolle, S. Callé, S. Dos Santos, O. Bou Matar, A two-dimensional pseudospectral model for time reversal and nonlinear elastic wave spectroscopy, J. Acoust. Soc. Am. 122 (6) (2007) 3220–3229.
[14] K. Van Den Abeele, F. Schubert, V. Aleshin, F. Windels, J. Carmeliet, Resonant bar simulations in media with localized damage, Ultrasonics 42 (2004) 1017–1024.
[15] A.S. Gliozzi, M. Nobili, M. Scalerandi, Localized nonlinear damage and analysis of its influence on resonance frequencies, J. Phys. D: Appl. Phys. 39 (2006) 3895–3903.
[16] I. Solodov, G. Busse, Nonlinear air-coupled emission: the signature to reveal and image microdamage in solid materials, Appl. Phys. Lett. 91 (25) (2007) 251910.
[17] T.J. Ulrich, P.A. Johnson, R.A. Guyer, Interaction dynamics of elastic waves with a complex nonlinear scatterer through the use of a time reversal mirror, Phys. Rev. Lett. 98 (2007) 104301(1–4).
[18] K. van den Abeele, J. Carmeliet, J.A. TenCate, P.A. Johnson, Nonlinear Elastic Wave Spectroscopy (NEWS) techniques to discern material damage, Part II: single-mode nonlinear resonance acoustic spectroscopy, Res. Nondestruct. Eval. 12 (1) (2000) 31–42.
[19] J.C. Lacouture, P.A. Johnson, F. Cohen-Tenoudji, Study of critical behavior in concrete during curing by application of dynamic linear and nonlinear means, J. Acoust. Soc. Am. 113 (3) (2003) 1325–1332.
[20] A.S. Gliozzi, M. Griffa, M. Scalerandi, Efficiency of time reversed acoustics for nonlinear damage detection in solids, J. Acoust. Soc. Am. 120 (2006) 2506–2517.
[21] S.A. Abo-Qudais, Effect of concrete mixing parameters on propagation of ultrasonic waves, Constr. Build. Mater. 19 (2005) 257–263.
[22] K. van den Abeele, A. Sutin, J. Carmeliet, P.A. Johnson, Micro-damage diagnostics using nonlinear elastic wave spectroscopy (NEWS), NDT E Int. 34 (2001) 239–248.
[23] M. Meo, G. Zumpano, Nonlinear elastic wave spectroscopy identification of impact damage on a sandwich plate, Compos. Struct. 71 (2005) 469–474.
[24] F. Barpi, S. Valente, Lifetime evaluation of concrete structures under sustained post-peak loading, Eng. Fract. Mech. 27 (2005) 2427–2443.
[25] K. Maekawa, K.F. El-Kashif, Cyclic cumulative damaging of reinforced concrete in post-peak regions, J. Adv. Concr. Technol. 2 (2) (2004) 257–271.
[26] S. Yuyama, Z.-W. Li, M. Yoshizawa, T. Tomokiyo, T. Uomoto, Evaluation of fatigue damage in reinforced concrete slab by acoustic emission, NDT E Int. 34 (2001) 381–387.